HHS Public Access

Author manuscript

Science. Author manuscript; available in PMC 2019 January 03.

Published in final edited form as:

Science. 2018 August 10; 361(6402): 599–603. doi:10.1126/science.aap9331.

Lacteal junction zippering protects against diet-induced obesity

Feng Zhang[1], **Georgia Zarkada**[1], **Jinah Han**[1], **Jinyu Li**[1], **Alexandre Dubrac**[1], **Roxana Ola**[1,2], **Gael Genet**[1], **Kevin Boyé**[1], **Pauline Michon**[1,3], **Steffen E. Künzel**[1], **Joao Paulo Camporez**[4], **Abhishek K. Singh**[5], **Guo-Hua Fong**[6], **Michael Simons**[1], **Patrick Tso**[7], **Carlos Fernández-Hernando**[5], **Gerald I. Shulman**[4,8], **William C. Sessa**[9], and **Anne Eichmann**[1,3,8,*]

[1]Cardiovascular Research Center, Yale University School of Medicine, New Haven, CT 06510-3221, USA.

[2]Department of Basic, Preventive and Clinical Science, University of Transylvania, 500019 Brasov, Romania

[3]INSERM U970, Paris Cardiovascular Research Center, 75015 Paris, France.

[4]Department of Internal Medicine, Yale University School of Medicine.

[5]Departments of Comparative Medicine and Pathology, Vascular Biology and Therapeutics Program and Integrative Cell Signaling and Neurobiology of Metabolism Program, Yale University School of Medicine.

[6]Department of Cell Biology, University of Connecticut Health Center, Farmington, CT, 06030-3501, USA.

[7]Department of Pathology and Laboratory Medicine, Metabolic Diseases Institute, University of Cincinnati, Galbraith Road, Cincinnati 45237-0507, USA.

[8]Department of Cellular and Molecular Physiology, Yale University School of Medicine.

[9]Department of Pharmacology, Vascular Biology and Therapeutics Program, Yale University School of Medicine.

Abstract

Excess dietary lipid uptake causes obesity, a major global health problem. Enterocyte-absorbed lipids are packaged into chylomicrons, which enter the bloodstream through intestinal lymphatic vessels called lacteals. Here, we show that preventing lacteal chylomicron uptake by inducible endothelial genetic deletion of *Neuropilin1* (*Nrp1*) and Vascular endothelial growth factor receptor 1 (*Flt1*) renders mice resistant to diet-induced obesity. Absence of NRP1 and FLT1 receptors increased VEGF-A bioavailability and signaling through VEGFR2, inducing lacteal junction zippering and chylomicron malabsorption. Restoring permeable lacteal junctions by VEGFR2 and

*Correspondence should be addressed to A.E. (anne.eichmann@yale.edu).

Author contributions: FZ, GZ, JH, JL, AD, RO, GG, KB, PM, SEK, JPC and AKS performed experiments and analyzed data. AE and FZ designed experiments, analyzed data and wrote the manuscript. GHF, MS, PT, CFH, WCS and GIS provided reagents or expertise.

Competing interests: Anne Eichmann and Feng Zhang are inventors on patent application (U.S. Provisional Application No. 62/686,140) submitted by Yale University that covers compositions and methods for preventing dietary lipid uptake and obesity.

Data and materials availability: All data is available in the manuscript or the supplementary materials.

Vascular endothelial (VE)-cadherin signaling inhibition rescued chylomicron transport in the mutant mice. Zippering of lacteal junctions by disassembly of cytoskeletal VE-cadherin anchors prevented chylomicron uptake in wildtype mice. These data suggest lacteal junctions may be targets to prevent dietary fat uptake.

Dietary fats are absorbed by enterocytes and incorporated into triglyceride-rich lipoproteins, called chylomicrons. Nearly all dietary lipids are transported in chylomicrons from the intestine to tissues via the lymphatic system. Chylomicrons enter the lymphatics through lacteals; specialized lymphatic capillaries located in the center of the intestinal villi. From there, they are transported through the mesenteric lymphatic vessels into the thoracic duct, which drains into the venous circulation, and become metabolized by the liver (1-3).

Preventing lacteal growth in mice by conditional deletion of the genes encoding *Vegf-c* or *Delta-like 4* (*Dll4*) renders mice resistant to high fat diet (HFD)-induced obesity, providing experimental evidence that lacteals could be targeted to prevent obesity (4,5). The cellular mechanisms controlling chylomicron entry into the lacteals are poorly understood: some studies suggested that chylomicrons enter through junctions between lymphatic endothelial cells (LECs) lining the lacteals (5-7), but other studies have shown they pass through LECs by transcytosis (3). The molecular mechanisms controlling lacteal chylomicron uptake are currently unknown. Here we show that chylomicron uptake is controlled by VEGF-A signaling, through modulation of lacteal junctions. Lacteals respond to high VEGF-A levels by zippering up their junctions, which impairs chylomicron passage and renders mice resistant to diet-induced obesity.

FLT1 and NRP1 are VEGF-A receptors that were previously implicated in metabolism regulation, but how they function in endothelium in this context remained undefined (fig.S1). We therefore generated pan-endothelial deletions of *Nrp1* and *Flt1* by crossing $Nrp1^{fl/fl}$ and $Flt1^{fl/fl}$ mice to $Cdh5\text{-}Cre^{ERT2}$ mice, where gene deletion can be induced by tamoxifen (TAM) in cells expressing the vascular endothelial cadherin promoter (hereafter referred to as *Nrp1;Flt1iECko* mice). Adult 5-week-old males and Cre-negative littermate controls received TAM to induce efficient gene deletion in the endothelium, as confirmed by Western blot and real-time qPCR on purified endothelial cells (fig.S2). HFD feeding was initiated at week 8 and continued for 16 weeks (wk) (fig.S2). Control mice doubled their body weight after 16wk of HFD feeding, while *Nrp1;Flt1iECko* mice gained little weight (Fig.1A-C). No weight differences were observed in mice on normal chow (Fig.1D). The weight of *Nrp1iECko* mice was similar to littermate controls (Fig.1E), while weight gain in *Flt1* single mutants was slightly reduced, and attributed to increased adipose tissue angiogenesis (8,9) (Fig.1F) as described previously.

HFD-fed *Nrp1;Flt1iECko* mice had reduced fat and increased lean body mass ratios when compared to control littermates and their body composition resembled lean control mice on normal chow (Fig.1G, fig.S3). In contrast to controls, *Nrp1;Flt1iECko* mice had reduced liver triglyceride content and did not develop hepatic steatosis after 8wk of HFD feeding (Fig.1H, fig.S4). *Nrp1;Flt1iECko* and control mice showed similar food and water consumption, physical activity, O_2 consumption, CO_2 production and energy expenditure

after 2wk and 8wk of HFD feeding (Fig.1I, fig.S5). Glucose tolerance in *Nrp1;Flt1iECko* mice was improved compared to controls (Fig.1J).

Plasma triglycerides, total cholesterol and high-density lipoprotein cholesterol (HDL) levels were reduced in *Nrp1;Flt1iECko* mice when compared to controls after 16wk on HFD (Fig. 2A), indicating that resistance to diet induced obesity was either due to defective lipid uptake into the bloodstream, reduction in very-low density lipoprotein (VLDL) production or to enhanced VLDL and chylomicron catabolism. To determine if lipid uptake was affected, we measured plasma triglyceride uptake following intra-gastric gavage with olive oil in the presence or absence of the lipoprotein lipase (LPL) inhibitor TritonWR1339. As expected, circulating triglyceride levels increased in controls in both conditions, but the effect was abrogated in *Nrp1;Flt1iECko* mice (Fig.2B-C). Similar results were obtained when we injected the mice with the LPL inhibitor Poloxamer 407 and gavaged with oil mixed with [^{3}H]-triolein (Fig.2D), indicating that absence of NRP1 and FLT1 attenuates fat absorption. Bomb calorimetry showed increased calorie content in the feces of *Nrp1;Flt1iECko* mice, suggesting that part of the lipid is not absorbed but rather cleared in the feces (Fig.2E). Histological analysis revealed the presence of oil-red-O labeled lipid particles in the *Nrp1;Flt1iECko* colon, whereas less lipid was present in the control colon (fig.S6). We confirmed reduced intestinal lipid uptake in *Nrp1;Flt1iECko* mice by analyzing postnatal day 7 (P7) mesenteries, after neonatal gene deletion. Chylomicrons were present in the mesenteric lymphatic vessels of control mice and single *Nrp1* or *Flt1* ko mice, but few lymphatic vessels containing milky chyle could be seen in *Nrp1;Flt1iECko* pups (Fig.2F, fig.S7). Neonatal *Nrp1;Flt1iECko* mice had decreased weight gain (fig.S8), which is consistent with lipid malabsorption.

Expression of key enzymes and components required for chylomicron assembly, including *Mtp, ApoB, Sar1b, Plagl2* and fatty acid transporters (*CD36*and *Fabps*), was similar in the jejunum of *Nrp1;Flt1iECko* and control mice, indicating that the enterocytes devoid of both *Nrp1 and Flt1* are able to assemble and secrete chylomicrons (fig.S9). Transmission electron microscopy (TEM) showed similar morphology of intestinal enterocytes and presence of chylomicrons within enterocytes and in the interstitial space between capillaries and lacteals regardless of genotype (Fig.2G, fig.S10). TEM also revealed the presence of lacteal LECs but strikingly, the lacteal lumen was almost completely lacking chylomicrons in *Nrp1;Flt1iECko* animals, while numerous chylomicrons were present within the lacteal lumen in controls (Fig.2G, fig.S10). High magnification views showed many open junctions between LECs in controls, but more closed LEC junctions in *Nrp1;Flt1iECko* mice (Fig.2G, fig.S10). These data are consistent with the concept that altered lacteal junctions results in defective lacteal chylomicron uptake, which limits weight gain in the absence of both NRP1 and FLT1.

Immunostaining of lacteal junctions with VE-cadherin confirmed that *Nrp1;Flt1iECko* mice exhibited fewer button-like LEC junctions and developed more impermeable zipper junctions compared to controls (Fig.3A-B). Lacteals devoid of both *Nrp1* and *Flt1* were of similar length, but showed reduced width compared to those lacking either *Nrp1* and *Flt1* alone, or control animals (fig.S11). VE-cadherin staining also revealed enlarged villus capillaries and disrupted BEC junctions, leading to leakage of intravenously injected

fluorescent dextran in *Nrp1;Flt1iECko* mice (Fig.3C-D, fig.S12). Postnatal or adult deletion of both *Nrp1* and *Flt1* caused altered vascular morphology and villus edema, which was surprisingly well tolerated and did not compromise vascular or enterocyte ultrastructure even after prolonged HFD feeding (fig.S10). Staining for pericytes, smooth muscle cells and macrophages, and analysis of inflammatory marker expression revealed no changes between controls and *Nrp1;Flt1iECko* mutants (fig.S13), suggesting a primary effect upon villus vasculature by the absence of *Nrp1* and *Flt1.*

Loss of junctional VE-cadherin staining in BECs is a hallmark of increased VEGF-A signaling (10), and FLT1 is a known VEGF-A decoy receptor (11). To test if loss of NRP1 and FLT1 increased intestinal VEGF-A signaling, we probed lysates from control and *Nrp1;Flt1iECko* tissues with antibodies against phosphorylated and total VEGFR2. Activation of both Y1173 and Y949 signaling was significantly increased in the absence of both *Nrp1 and Flt1* when compared to control littermates or single *Flt1iECko* mice (Fig.3E, fig.S14), indicating that NRP1 enhances FLT1 decoy function. NRP1 also acts as a VEGFR2 co-receptor to activate downstream ERK signaling (12), and ERK activation was accordingly deficient in most *Nrp1;Flt1iECko* tissues (fig.S14).

Loss of *Flt1* has been shown to induce adipose tissue browning (8,9) and we observed increased vascular density in white adipose tissue (WAT) but not in brown adipose tissue (BAT) in *Nrp1;Flt1iECko* mice (fig.S15). Expression levels of the mitochondrial uncoupling protein UCP1 were only slightly increased in *Nrp1;Flt1iECko* epididymal WAT, and were unchanged in subcutaneous WAT and BAT (fig.S15). Thus, adipose tissue browning is unlikely to account for resistance to diet-induced obesity in *Nrp1;Flt1iECko* animals.

VEGF-A is known to increase blood-vascular permeability (13,14) and lacteals express VEGFR2 (fig.S16), but effects of VEGF-A on lacteal junctions have previously not been investigated, to the best of our knowledge. Intravenous VEGF-A injection disrupted BEC junctions after 30min as expected, but also increased the number of zipper-like junctions in lacteals (Fig.3F-G). Intravenous injection of the lymphatic growth factor VEGF-C also increased junction zippering, but to a lesser extent than VEGF-A, while a mutant VEGF-C-156S protein that cannot bind VEGFR2 (15) had no effect (Fig.3G, fig.S16). *In vitro,* treatment of starved confluent LECs with VEGF-A and VEGF-C, but not VEGF-C-156S, promoted the appearance of straighter VE-cadherin lined junctions and decreased actin stress fiber anchoring to perpendicular arranged VE-cadherin (fig.S16). These data suggested that increased VEGF-A/VEGFR2 signaling in *Nrp1;Flt1iECko* villi might cause defective chylomicron uptake via lacteal junction zippering.

Intestinal villi show high levels of *Vegf-a* expression, lower levels of *Vegf-c* and little expression of *Vegf-b* (fig.S17). Expression of *Flt1* is increased at birth, concomitantly with the expression of *Mtp* and *ApoB,* a known inducer of *Flt1* (16) (fig.S17). RNA sequencing showed that mature intestinal BECs express four times as many copies of *Nrp1* when compared to *Flt1* (fig.S17), consistent with the concept that chylomicrons induce an increase of FLT1, which functions together with NRP1 to prevent excessive VEGF-A signaling, thereby allowing lacteal junction maturation and chylomicron absorption.

Cdh5-Cre^{ERT2} mediates gene deletion in both intestinal BECs and LECs, raising the possibility that NRP1;FLT1 function might be required in both compartments in a cell-autonomous manner. We therefore generated LEC-specific *Nrp1* and *Flt1* deletions using *Prox1-Cre*$^{ERT2(BAC)}$ mice. *Prox1-Cre*$^{ERT2(BAC)}$ specifically recombined mesenteric and lacteal LECs, but loss of *Nrp1;Flt1* in LECs had no detectable effects on postnatal mesenteric chyle uptake or on weight gain in adult HFD-fed mice (fig.S18). Lymphatic button-like junctions were present and responded to VEGF-A by forming zippers (fig.S18). Together with highly enriched expression of *Nrp1* and *Flt1* in intestinal BECs compared to LECs (17), these data suggest that NRP1 and FLT1 function in villus BECs to antagonize VEGF-A/VEGFR2 signaling on lacteal LECs.

Interestingly, the effect of *Nrp1;Flt1* deletion on LEC junctions was tissue-specific, as the junction morphology in initial lymphatics in the skin and diaphragm of *Nrp1;Flt1iECko* mice was similar to controls (fig.S19). Intravenous VEGF-A, but not VEGF-C or VEGF-C-156S, modestly increased dermal initial lymphatic junction zippering (fig.S19). However, intradermal injection of VEGF-A or VEGF-C robustly increased dermal LEC junction zippering, while VEGF-C-156S did not (fig.S19). High VEGFR2 signaling may therefore be a general inducer of lymphatic junction zippering, which is antagonized by NRP1;FLT1 decoys in the small intestine, and via other mechanisms in other tissues.

If enhanced VEGF-A signaling accounted for defective chylomicron uptake in *Nrp1;Flt1iECko* mice, blocking VEGFR2 function should rescue this process. Indeed, intraperitoneal injection of the VEGFR2 blocking antibody DC101 (18) decreased VEGFR2 phosphorylation, and increased uptake of mesenteric chyle in neonates 6h after treatment (Fig.4A-B, fig.S20). Dilation of villus capillaries was reduced, and width of lacteals increased (fig.S20). DC101 treated double mutants showed less dextran leak from intestinal capillaries (fig.S20), had more LEC button-like junctions and fewer zippers, and higher plasma lipid levels in the bloodstream when compared to untreated *Nrp1;Flt1iECko* animals (Fig.4C-D).

We next determined if changes in lacteal junctions were sufficient to impair chylomicron uptake. Button-like junctions develop postnatally by transformation of zipper-like junctions in a poorly characterized mechanism that involves Angiopoietin2 (ANGPT2) and changes in plasma membrane localization of VE-cadherin and LYVE-1 (19-21). LYVE-1 immunostaining and protein levels of LYVE-1 and ANGPT2 were comparable between *Nrp1;Flt1iECko* mutants and controls, and inhibition of MMP-mediated LYVE-1 cleavage (22) had no effect on mesenteric chylomicron uptake (fig.S21). To test VE-cadherin function we used the BV13 antibody, which disrupts endothelial adherens junctions in BECs and LECs (19). Intraperitoneal injection of 10μg/g BV13 into postnatal mice rescued lacteal chylomicron uptake into mesenteric lymphatics in *Nrp1;Flt1iECko* mutants and disrupted LEC junctions (Fig.4E-F, fig.S22). Importantly, BV13 treatment disrupted capillary BEC adherens junctions but did not affect chylomicron uptake in control mice (fig.S22). This indicates that disruption of BEC junctions per se has no effect on chylomicron transport and that lacteal LEC junctions, but not capillary BEC junctions, control chylomicron uptake.

In a complementary approach, we treated *Nrp1;Flt1iECko* mice with dexamethasone, a drug that induces zipper to button-like junction transition in tracheal lymphatics (21). Short-term dexamethasone treatment decreased the number of zipper-like junctions and increased chyle uptake in mesenteries of a subset of *Nrp1;Flt1iECko* mice (fig.S23). *Nrp1;Flt1iECko* mutant BEC junctions were unaffected by dexamethasone, but treated mutant animals exhibited fewer zipper-like junctions (fig.S23), confirming that LEC but not BEC junctional changes correlate with chylomicron uptake.

We reasoned that junctional changes between continuous VE-cadherin lined zippers and discontinuous buttons could depend on cytoskeletal VE-cadherin anchoring, which can be inhibited in BECs by antagonizing Rho GTPase signaling (23). Indeed, the ROCK inhibitor Y27632 induced straighter junctions of cultured LECs *in vitro* (fig.S24), and short-term treatment of wildtype mice with Y27632 reduced chylomicron transport to mesenteric lymphatics and increased lacteal junction zippering, without affecting BEC junctions (Fig. 4G-H, fig.S24). TEM showed open lacteal junctions and chylomicrons in the lacteal lumen of untreated mice, but closed junctions and almost no chylomicrons in the lacteal lumen in Y27632 treated mice (Fig.4I).

Together, we demonstrate that high VEGF-A signaling has opposing effects on blood and lymphatic vessels: opening capillary cell-cell junctions via well-studied pathways (10,24), but closing lymphatic junctions via transformation of buttons into zippers. We show that LEC VEGFR2 activation inhibits VE-cadherin cytoskeletal anchoring, which can be mimicked by ROCK inhibition *in vitro* and *in vivo.* Cytoskeletal VE-cadherin anchoring might generate pulling forces that help maintain lacteal button junctions open. Importantly, we show that short-term effects of VEGF-A gain of function (over hours instead of days) (25) is sufficient to functionally switch junction morphology and lipid uptake. This reveals an intestinal-specific lacteal barrier that could be closed on demand to prevent lipid uptake (Fig.4J). Thus, NRP1 and FLT1 appear to function collaboratively as a double decoy receptor system in intestinal BECs to limit VEGF-A signaling (Fig.4J). VEGF-A/VEGFR2 signaling might provide a LEC growth signal together with VEGF-C/VEGFR3 (21,26). In addition, VEGFR2 signaling acts as a physiological inhibitor of lacteal maturation, whose activity must be dampened to allow acquisition of transport function. This mechanism may also apply to other tissues, with implications for edema prevention. Full knowledge of the mechanism responsible for LEC junction zippering holds promise for the identification of molecular targets for the treatment of obesity. Of note, ROCK inhibitors are clinically approved for treatment of cerebral vasospasm in some countries and have been shown to improve metabolism and decrease obesity in rodent models (27-30). Further studies of the effects of such drugs in obesity prevention, as well as of potential adverse effects of lacteal junction zippering on intestinal health are warranted.

Supplementary Material

Refer to Web version on PubMed Central for supplementary material.

Acknowledgments:

We thank Yale Mouse Metabolic Phenotyping Center, Yale Electron Microscopy Facility, and Cincinnati Mouse Metabolic Phenotyping Center for assistance, Mr. Y. Zhao for ANCOVA analysis and Drs. K. Alitalo, J-L. Thomas and S. Lee for discussion.

Funding: This study was supported by grants from NHLBI (1R01HLI125811), NEI (1R01EY025979-01, P30 EY026878) and Agence nationale de la recherche (ANR Brainwash) to AE. FZ was supported by a T32 grant from NHLBI (2T32HL7950-16A1). GZ was supported by an EMBO Long-Term fellowship (ALTF 87-2016) and a T32 grant from NHLBI (2T32HL007974-16). AD and RO were supported by AHA postdoctoral fellowships 14POST20380207 and 15POST25560114, respectively. MS was supported by NIH grants R01HL053793 and P01HL107205 to MS.

References and Notes:

1. Bernier-Latmani J, Petrova TV, Intestinal lymphatic vasculature: structure, mechanisms and functions. Nat Rev Gastroenterol Hepatol 14, 510–526 (2017). [PubMed: 28655884]
2. Randolph GJ, Miller NE, Lymphatic transport of high-density lipoproteins and chylomicrons. J Clin Invest 124, 929–935 (2014). [PubMed: 24590278]
3. Dixon JB, Mechanisms of chylomicron uptake into lacteals. Ann N Y Acad Sci 1207 Suppl 1, E52–57 (2010). [PubMed: 20961306]
4. Nurmi H et al., VEGF-C is required for intestinal lymphatic vessel maintenance and lipid absorption. EMBO molecular medicine 7, 1418–1425 (2015). [PubMed: 26459520]
5. Bernier-Latmani J et al., DLL4 promotes continuous adult intestinal lacteal regeneration and dietary fat transport. J Clin Invest 125, 4572–4586 (2015). [PubMed: 26529256]
6. Casley-Smith JR, The identification of chylomicra and lipoproteins in tissue sections and their passage into jejunal lacteals. J Cell Biol 15, 259–277 (1962). [PubMed: 14019085]
7. Sabesin SM, Frase S, Electron microscopic studies of the assembly, intracellular transport, and secretion of chylomicrons by rat intestine. J Lipid Res 18, 496–511 (1977). [PubMed: 894141]
8. Robciuc MR et al., VEGFB/VEGFR1-Induced Expansion of Adipose Vasculature Counteracts Obesity and Related Metabolic Complications. Cell Metab 23, 712–724 (2016). [PubMed: 27076080]
9. Seki T et al., Ablation of endothelial VEGFR1 improves metabolic dysfunction by inducing adipose tissue browning. J Exp Med 215, 611–626 (2018). [PubMed: 29305395]
10. Simons M, Gordon E, Claesson-Welsh L, Mechanisms and regulation of endothelial VEGF receptor signalling. Nat Rev Mol Cell Biol 17, 611–625 (2016). [PubMed: 27461391]
11. Ambati BK et al., Corneal avascularity is due to soluble VEGF receptor-1. Nature 443, 993–997 (2006). [PubMed: 17051153]
12. Lanahan A et al., The neuropilin 1 cytoplasmic domain is required for VEGF-A-dependent arteriogenesis. Dev Cell 25, 156–168 (2013). [PubMed: 23639442]
13. Sun Z et al., VEGFR2 induces c-Src signaling and vascular permeability in vivo via the adaptor protein TSAd. J Exp Med 209, 1363–1377 (2012). [PubMed: 22689825]
14. Li X et al., VEGFR2 pY949 signalling regulates adherens junction integrity and metastatic spread. Nat Commun 7, 11017 (2016). [PubMed: 27005951]
15. Joukov V et al., A recombinant mutant vascular endothelial growth factor-C that has lost vascular endothelial growth factor receptor-2 binding, activation, and vascular permeability activities. J Biol Chem 273, 6599–6602 (1998). [PubMed: 9506953]
16. Avraham-Davidi I et al., ApoB-containing lipoproteins regulate angiogenesis by modulating expression of VEGF receptor 1. Nat Med 18, 967–973 (2012). [PubMed: 22581286]
17. Jurisic G et al., An unexpected role of semaphorin3a-neuropilin-1 signaling in lymphatic vessel maturation and valve formation. Circ Res 111, 426–436 (2012). [PubMed: 22723300]
18. Prewett M et al., Antivascular endothelial growth factor receptor (fetal liver kinase 1) monoclonal antibody inhibits tumor angiogenesis and growth of several mouse and human tumors. Cancer Res 59, 5209–5218 (1999). [PubMed: 10537299]

19. Baluk P et al., Functionally specialized junctions between endothelial cells of lymphatic vessels. J Exp Med 204, 2349–2362 (2007). [PubMed: 17846148]
20. Zheng W et al., Angiopoietin 2 regulates the transformation and integrity of lymphatic endothelial cell junctions. Genes Dev 28, 1592–1603 (2014). [PubMed: 25030698]
21. Yao LC, Baluk P, Srinivasan RS, Oliver G, McDonald DM, Plasticity of button-like junctions in the endothelium of airway lymphatics in development and inflammation. Am J Pathol 180, 2561–2575 (2012). [PubMed: 22538088]
22. Wong HL et al., MT1-MMP sheds LYVE-1 on lymphatic endothelial cells and suppresses VEGF-C production to inhibit lymphangiogenesis. Nat Commun 7, 10824 (2016). [PubMed: 26926389]
23. Huveneers S et al., Vinculin associates with endothelial VE-cadherin junctions to control force-dependent remodeling. J Cell Biol 196, 641–652 (2012). [PubMed: 22391038]
24. Dorland YL, Huveneers S, Cell-cell junctional mechanotransduction in endothelial remodeling. Cell Mol Life Sci 74, 279–292 (2017). [PubMed: 27506620]
25. Schlieve CR et al., Vascular Endothelial Growth Factor (VEGF) Bioavailability Regulates Angiogenesis and Intestinal Stem and Progenitor Cell Proliferation during Postnatal Small Intestinal Development. PLoS One 11, e0151396 (2016). [PubMed: 26978773]
26. Wirzenius M et al., Distinct vascular endothelial growth factor signals for lymphatic vessel enlargement and sprouting. J Exp Med 204, 1431–1440 (2007). [PubMed: 17535974]
27. Shibuya M et al., Effect of AT877 on cerebral vasospasm after aneurysmal subarachnoid hemorrhage. Results of a prospective placebo-controlled double-blind trial. J Neurosurg 76, 571–577 (1992). [PubMed: 1545249]
28. Kikuchi Y et al., A Rho-kinase inhibitor, fasudil, prevents development of diabetes and nephropathy in insulin-resistant diabetic rats. J Endocrinol 192, 595–603 (2007). [PubMed: 17332527]
29. Tokuyama H et al., Role of mineralocorticoid receptor/Rho/Rho-kinase pathway in obesity-related renal injury. Int J Obes (Lond) 36, 1062–1071 (2012).
30. Okin D, Medzhitov R, The Effect of Sustained Inflammation on Hepatic Mevalonate Pathway Results in Hyperglycemia. Cell 165, 343–356 (2016). [PubMed: 26997483]
31. Gu C et al., Neuropilin-1 conveys semaphorin and VEGF signaling during neural and cardiovascular development. Dev Cell 5, 45–57 (2003). [PubMed: 12852851]
32. Ho VC, Duan LJ, Cronin C, Liang BT, Fong GH, Elevated vascular endothelial growth factor receptor-2 abundance contributes to increased angiogenesis in vascular endothelial growth factor receptor-1-deficient mice. Circulation 126, 741–752 (2012). [PubMed: 22753193]
33. Wang Y et al., Ephrin-B2 controls VEGF-induced angiogenesis and lymphangiogenesis. Nature 465, 483–486 (2010). [PubMed: 20445537]
34. Bazigou E et al., Genes regulating lymphangiogenesis control venous valve formation and maintenance in mice. J Clin Invest 121, 2984–2992 (2011). [PubMed: 21765212]
35. Tschop MH et al., A guide to analysis of mouse energy metabolism. Nat Methods 9, 57–63 (2011). [PubMed: 22205519]
36. Otway S, Robinson DS, The effect of a non-ionic detergent (Triton WR 1339) on the removal of triglyceride fatty acids from the blood of the rat. J Physiol 190, 309–319 (1967). [PubMed: 6049000]
37. Johnston TP, The P-407-induced murine model of dose-controlled hyperlipidemia and atherosclerosis: a review of findings to date. J Cardiovasc Pharmacol 43, 595–606 (2004). [PubMed: 15085072]
38. Eichmann A, Simons M, VEGF signaling inside vascular endothelial cells and beyond. Curr Opin Cell Biol 24, 188–193 (2012). [PubMed: 22366328]
39. Joukov V et al., Proteolytic processing regulates receptor specificity and activity of VEGF-C. EMBO J 16, 3898–3911 (1997). [PubMed: 9233800]
40. Hagberg CE et al., Vascular endothelial growth factor B controls endothelial fatty acid uptake. Nature 464, 917–921 (2010). [PubMed: 20228789]
41. Hagberg CE et al., Targeting VEGF-B as a novel treatment for insulin resistance and type 2 diabetes. Nature 490, 426–430 (2012). [PubMed: 23023133]

42. Lahteenvuo JE et al., Vascular endothelial growth factor-B induces myocardium-specific angiogenesis and arteriogenesis via vascular endothelial growth factor receptor-1-and neuropilin receptor-1-dependent mechanisms. Circulation 119, 845–856 (2009). [PubMed: 19188502]
43. Dijkstra MH et al., Lack of cardiac and high-fat diet induced metabolic phenotypes in two independent strains of Vegf-b knockout mice. Sci Rep 4, 6238 (2014). [PubMed: 25168313]
44. Kivela R et al., VEGF-B-induced vascular growth leads to metabolic reprogramming and ischemia resistance in the heart. EMBO Mol Med 6, 307–321 (2014). [PubMed: 24448490]
45. Gelfand MV et al., Neuropilin-1 functions as a VEGFR2 co-receptor to guide developmental angiogenesis independent of ligand binding. Elife 3, e03720 (2014). [PubMed: 25244320]
46. Simons M, Eichmann A, Molecular controls of arterial morphogenesis. Circ Res 116, 1712–1724 (2015). [PubMed: 25953926]
47. Fantin A et al., NRP1 Regulates CDC42 Activation to Promote Filopodia Formation in Endothelial Tip Cells. Cell Rep 11, 1577–1590 (2015). [PubMed: 26051942]
48. Fantin A et al., NRP1 acts cell autonomously in endothelium to promote tip cell function during sprouting angiogenesis. Blood 121, 2352–2362 (2013). [PubMed: 23315162]
49. Aspalter IM et al., Alk1 and Alk5 inhibition by Nrp1 controls vascular sprouting downstream of Notch. Nat Commun 6, 7264 (2015). [PubMed: 26081042]
50. Wilson AM et al., Neuropilin-1 expression in adipose tissue macrophages protects against obesity and metabolic syndrome. Sci Immunol 3, eaan4626 (2018). [PubMed: 29549139]
51. Muzumdar MD, Tasic B, Miyamichi K, Li L, Luo L, A global double-fluorescent Cre reporter mouse. Genesis 45, 593–605 (2007). [PubMed: 17868096]

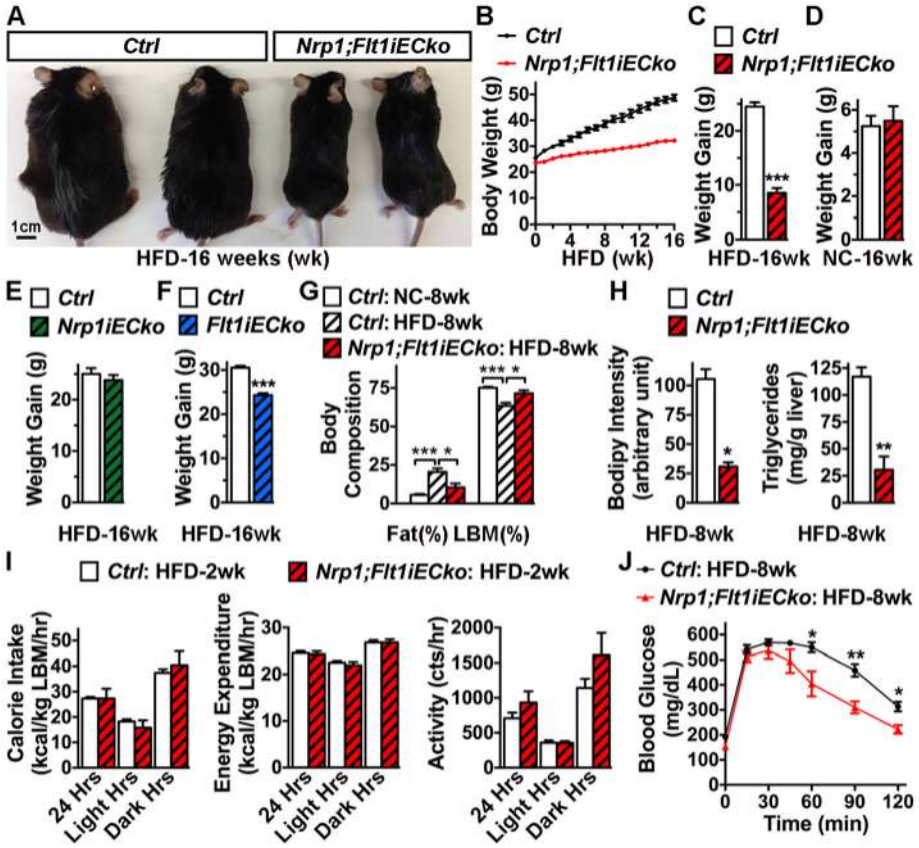

Fig.1. *Nrp1;Flt1iECko* mice are resistant to diet-induced obesity.

(**A**) *Nrp1;Flt1iECko* and *Cre*-negative littermate control (*Ctrl*) mice after 16wk HFD. (**B**-**C**) Growth curves (**B**) and weight gain (**C**) of *Ctrl* (n=8) and *Nrp1;Flt1iECko* (n=11) mice after 16wk HFD feeding. Data are mean±SEM. ***, p-0.001. Mann-Whitney U test. (**D**-**F**) Weight gain of normal chow (NC)- or HFD-fed mice (n=4-11/group). Data are mean±SEM. ***, p<0.001. Mann-Whitney U test. (**G**) Body composition of mice (n=7-8/group) after 8wk NC or HFD. Data are mean±SEM. * p<0.05, ***, p<0.001. Mann-Whitney U test. (**H**) Quantification of Bodipy staining intensity of liver cryosections (left) and liver triglyceride content (right) from 8wk HFD-fed mice (n=4-5/group). Data are mean±SEM. * p<0.05, ***, p<0.001. Mann-Whitney U test. (**I**) Calorie intake, energy expenditure and activity of *Ctrl* (n=7) and *Nrp1;Flt1iECko* (n=5) mice after 2wk on HFD. Data represent 24h, light cycle (7:00am-7:00pm) and dark cycle (7:00pm-7:00am) average, normalized to lean body mass (LBM). Error bars: SEM. (**J**) Intraperitoneal glucose tolerance test in HFD-fed *Ctrl* (n=10) and *Nrp1;Flt1iECko* (n=6) mice. Data are mean±SEM. *, p<0.05; **, p<0.01. Mann-Whitney U test.

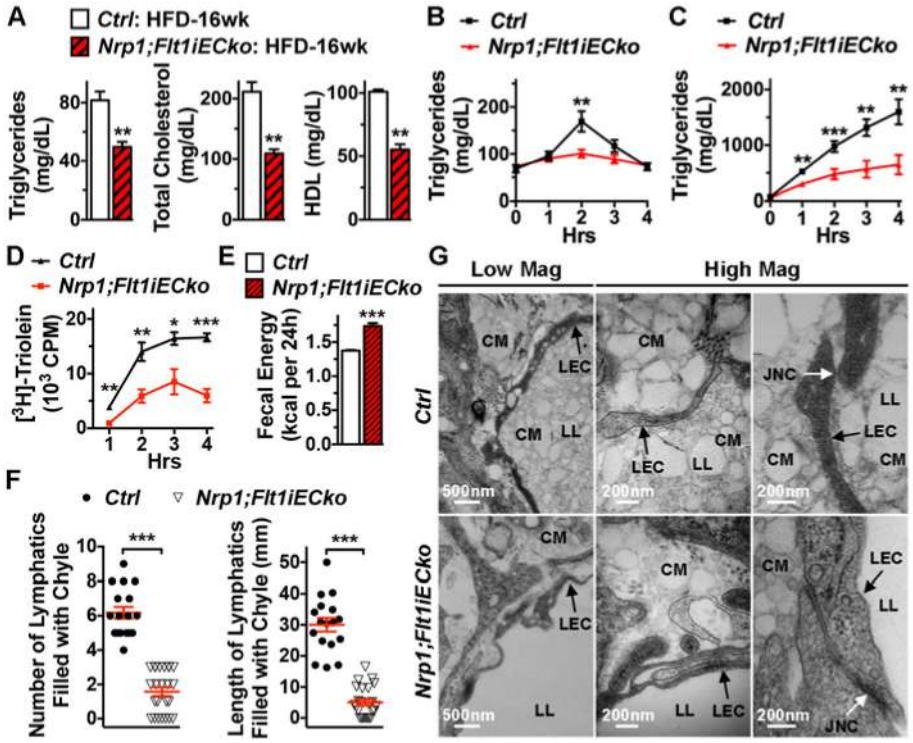

Fig.2. Endothelial *Nrp1;Flt1* deletion prevents lacteal chylomicron absorption.

(**A**) Plasma lipid profile in 6h fasted *Ctrl* (n=6) and *Nrp1;Flt1iECko* mice (n=6) after 16wk HFD. Data are mean±SEM. **, p<0.01. Mann-Whitney U test. (**B**-**C**) Plasma triglyceride content in NC-fed adult mice following gavage with 200μ1 olive oil. All mice (n=8-10/group) received 6h fasting and mice in (**C**) received Triton WR1339 (0.5g/kg) i.p. 30min prior to gavage. Data are mean±SEM. **, p<0.01, ***, p<0.001. Mann-Whitney U test. (**D**) Plasma ^{3}H CPM (counts per minute) in NC-fed adult mice after gavage with ^{3}H-triolein containing lipid. Mice (n=5/group) were fasted for 6h and injected i.p. with poloxamer 407 (1g/kg) 30min prior to gavage. Data are mean±SEM. *, p<0.05; **, p<0.01, ***, p<0.001. Mann-Whitney U test. (**E**) Fecal bomb calorimetry analysis of 2wk HFD-fed mice (n=8/group). Data are mean±SEM. ***, p<0.001. Mann-Whitney U test. (**F**) Quantifications of chyle-filled lymphatics in mesenteries of P7 mice after 3X100μg TAM injection at P2-P4. Each dot represents one mouse (n=17-24/group). Error bars: SEM. ***, p<0.001. Mann-Whitney U test. (**G**) Transmission electron microscopy of jejunum central lacteals in P13 mice. LL: lacteal lumen; LEC: lymphatic endothelial cell; CM: chylomicron. JNC: junction. Note closed LEC junction and empty lacteal lumen in *Nrp1;Flt1iECko* mice.

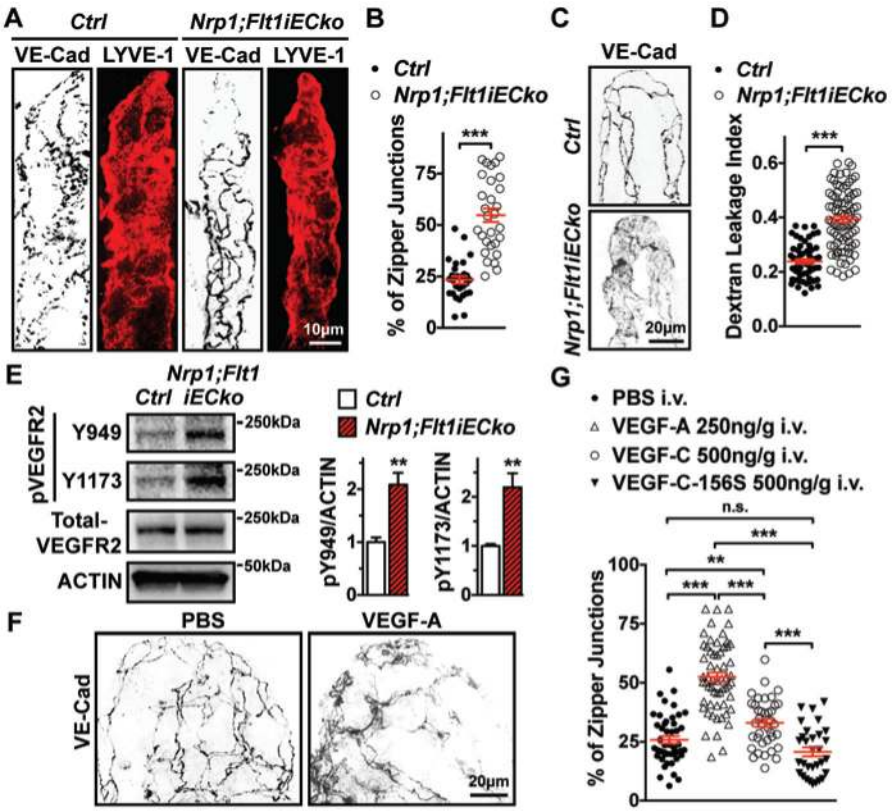

Fig.3. Increased VEGF-A signaling alters villus endothelial junctions.

(**A**) VE-Cad and LYVE-1 staining of whole-mounted jeunum lacteals from P13-P18 mice following postnatal TAM administration. (**B**) Quantification of zipper-like lacteal junctions in **A**. Each dot represents one lacteal (7 mice/group). Data are mean±SEM. ***, p<0.001. Mann-Whitney U test. (**C**) VE-Cad staining of whole-mounted jejunum BEC junctions from P7 mice. (**D**) Quantification of dextran leakage in P11 mice after Rhodamine-dextran and Alexa 647-IsoB4 i.v. injection for 10min. Each dot represents one villus (5-6 mice/group). Data are mean±SEM. ***, p<0.001. Mann-Whitney U test. (**E**) Western blots and quantifications of VEGFR2 phosphorylation in P7 jejunum lysates. n=5-6 mice/group. Data are mean±SEM. **, p<0.01. Mann-Whitney U test. (**F**-**G**) VE-Cad staining of villus BEC junctions and quantification of zipper-like lacteal junctions in jejunum from P18-P21 wildtype mice 30min after injection of growth factors or PBS. Each dot represents one lacteal (4-6 mice/group). Data are mean±SEM. n.s., not significant; **, p<0.01, ***, p<0.001. Mann-Whitney U test.

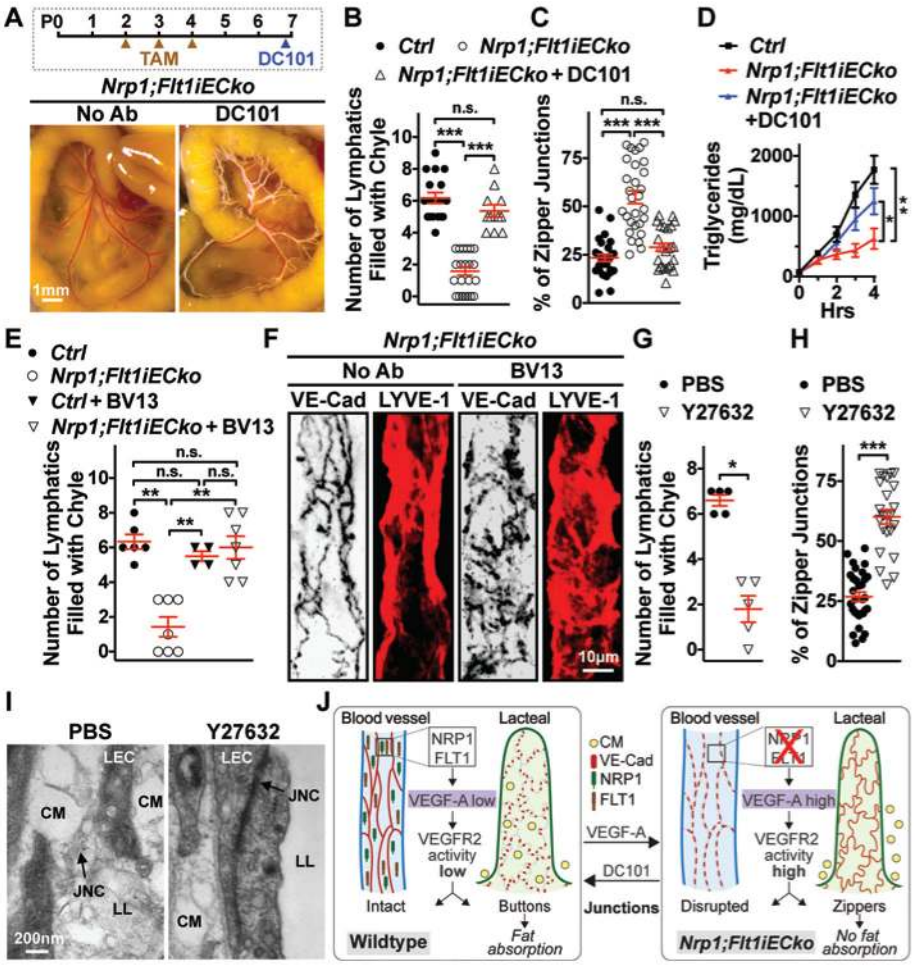

Fig.4. Lacteal zipper junctions prevent chylomicron absorption.

(**A**-**D**) DC101 rescues fat absorption in *Nrp1;Flt1iECko* mice. (**A**) Experimental timeline of TAM injection and DC101 treatment (30μg/g, i.p., for 6h) and mesenteries of P7 *Nrp1;Flt1iECko* mice with or without DC101. (**B**) Quantification of chyle-filled lymphatics in **A**. Each dot represents one mouse (n=11-24/group). Data are mean±SEM. n.s., not significant; ***, p<0.001. Mann-Whitney U test. (**C**) Quantification of zipper-like lacteal junctions in P13-P18 *Nrp1;Flt1iECko* jejunum with or without DC101. Each dot represents one lacteal (4-7 mice/group). Data are mean±SEM. n.s., not significant; ***, p<0.001. Mann-Whitney U test. (**D**) Plasma triglyceride content in NC-fed adult mice after 6h fasting and lipid gavage. All mice (n=5-8/group) received TritonWR1339 (0.5g/kg, i.p., 30 min prior to gavage) and some received DC101 (30μg/g, i.p. 4h prior to gavage). Data are mean ±SEM. *, p<0.05, **, p<0.01. Mann-Whitney U test. (**E**-**F**) BV13 rescues chylomicron uptake in *Nrp1;Flt1iECko* mice. (**E**) Quantification of chyle-filled lymphatics in P7 mice with or without BV13 treatment (10μg/g, i.p., for 4h). Each dot represents one mouse (n=5/group). Data show mean±SEM. n.s., not significant; **, p<0.01. Mann-Whitney U test. (**F**) VE-Cad and LYVE-1 staining of jejunum lacteals from P13 *Nrp1;Flt1iECko* mice with or without BV13. (**G**-**I**) ROCK inhibition prevents chylomicron uptake in wildtype mice. (**G**) Quantification of chyle-filled lymphatics in mesenteries of P10 mice treated with Y27632

(20μg/g, i.p., for 4h) or PBS. Each dot represents one mouse (n=5/group). Data are mean ±SEM. *, p<0.05. Mann-Whitney U test. (**H**) Quantification of zipper-like lacteal junctions in P13-15 mice treated with Y27632 or PBS. Each dot represents one lacteal (4 mice/group). Data are mean±SEM. ***, p<0.001. Mann-Whitney U test. (**I**) TEM analysis of lacteals in P13 mice with or without Y27632 treatment. LL: lacteal lumen; LEC: lymphatic endothelial cell; CM: chylomicron. JNC: junction. (**J**) Model of NRP1;FLT1 effects on BECs and LECs in intestinal villi. VEGF-A binding to NRP1;FLT1 on BECs limits VEGF-A bioavailability for VEGFR2, resulting in continuous and discontinuous cell junctions in BECs and LECs, respectively. Discontinuous button-like LEC junctions allow lacteal chylomicron uptake. Note that NRP1;FLT1 are only highly expressed on BECs. Increased VEGF-A concentrations or *Nrp1;Flt1* deletion in BECs result in excessive VEGFR2 activation, which disrupts BEC junctions while zippering up lacteal LEC junctions, thereby preventing chylomicron uptake. This phenotype can be rescued by inhibition of VEGFR2 signaling with DC101.